2012 Fourth International EURASIP Workshop on RFID Technology

Fast Algorithm for Leaking Carrier Canceller Adjustment

Gregor Lasser and Wolfgang Gartner
Vienna University of Technology
Institute of Telecommunications
gregor.lasser@nt.tuwien.ac.at

Robert Langwieser and Christoph F. Mecklenbräuker
Vienna University of Technology
Christian Doppler Laboratory
Wireless Technologies for Sustainable Mobility
cfm@nt.tuwien.ac.at

***Abstract*—RFID readers for passive tags generally suffer from self-interference. The transmitter of the RFID reader is also in operation during receive periods to power the tag and enable backscatter modulation. The state-of-the-art solution employs a leaking carrier canceller, which needs to be adjusted. The proposed fast algorithm provides a starting point for conventional gradient based approaches, which already improves isolation by $7.2\,\mathrm{dB}$ at least. It is based on three scalar measurements, and does not demand for special hardware. The algorithm was tested on our RFID testbed and experiments show a significant decrease of steps necessary to reach the final leaking carrier canceller setting.**

***Keywords*-RFID, leakage cancellation, carrier compensation, adjustment algorithm, CCU, LCC**

I. Introduction

Radio Frequency IDentification (RFID) systems for UHF and microwave frequencies can be classified in active and passive systems, depending on the type of tags they use. While active tags contain a transmitter to send data back to an RFID reader using radio waves, passive tags use backscatter modulation to transmit data to the reader. This approach requires a continuously transmitting RFID reader and a tag which modulates its antenna terminating impedance synchronous to the transmit data [1]. This change in antenna termination impedance results in a modulated differential radar cross section of the tag as defined in [2], which can be detected using a receiver operating at the same frequency as the transmitter, like in a conventional radar system. To avoid overloading or even destruction of the receiver due to the active transmitter for the passive tag case, isolation techniques based on single or dual antenna configurations are employed. Single antenna techniques rely on directional couplers or circulators to separate transmit and receive paths. Using separate antennas for transmit and receive provides some isolation, especially if directive antennas are mounted adequate with sufficient separation. However, both system designs may exhibit poor isolations which demand for expensive receiver architectures with high dynamic range. Several authors [3]–[9] and commercial reader chips [10] propose and use leaking carrier cancellation techniques to reduce the hardware demands and increase the RFID reader performance.

The principle of leakage cancellation is to extract a part of the transmit signal, adjust its amplitude to be equal and its phase to be opposite of the leakage signal, and add this leakage compensation signal to the receiver input signal. While this principal is simple, adjustment of the Leaking Carrier Canceller (LCC) is critical since a misadjusted LCC can even degrade the isolation. While some authors propose to use gradient based approaches [7], [10], employ vector amplitude detection [6], or even full scans of the LCC adjustment range [10], we propose a new fast algorithm which is based on only three scalar measurements.

In Section II the proposed algorithm is described in detail. Further, the measurement setup is described, which was used to validate the feasibility of the algorithm and analyse its performance in an actual RFID hardware. In Section IV three different types of measurements are presented. First, we propose a measurement self calibration routine used for all measurements. Then we present measurement results which demonstrate the feasibility of the proposed algorithm, based on randomly chosen artificial leakage signals. We continue with quantitative analysis of the reduction in number of steps required for a complete LCC alignment, when using the proposed fast algorithm as a starting point for a gradient search, when compared to a pure gradient search algorithm. Further, we evaluate the relative error of the proposed algorithm in the I/Q–plane when compared to a conventional gradient based algorithm . Finally, we present a measurement with a practical RFID scenario including antennas, both for a single and dual antenna scenario.

II. Algorithm

The proposed algorithm is based on three scalar amplitude measurements. Since every reader which employs a leaking carrier cancellation is equipped with a device to detect the amplitude or power of the input signal, no further hardware is required.

In the first step the LCC is switched off while the transmitter of the RFID reader remains switched on and generates a Continous Wave (CW) signal. The receiver input signal is due to leakage from transmitter to receiver, thus forming our unwanted leakage signal $\tilde{r}$ that we wish to cancel. A measurement of the amplitude of this input signal is performed, which can be written as:

$$r_0 = \sqrt{x^2 + y^2}, \tag{1}$$

978-0-7695-4813-5/12 $26.00 © 2012 IEEE
DOI 10.1109/RFID.2012.27

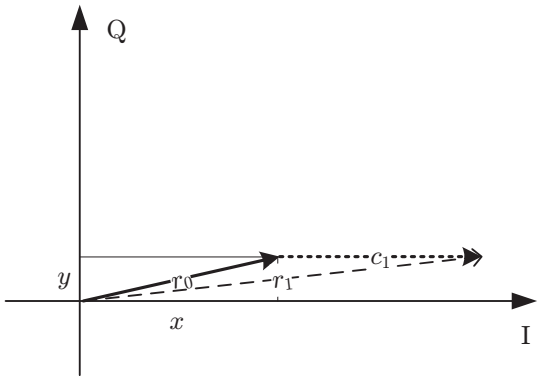

Figure 1. Illustration of the leaking signal and the measurement signal in the second step of the algorithm.

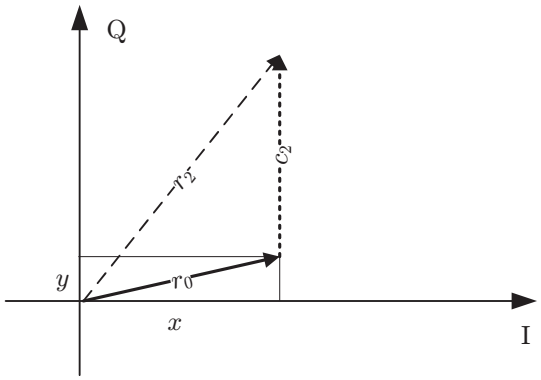

Figure 2. Illustration of the leaking signal and the measurement signal in the third step of the algorithm.

where x and y are the unknown inphase (I) and quadrature (Q) components of the undesired leakage signal $\tilde{r}$.

In the second step we switch on the LCC and apply an additional probing signal $\tilde{c_1}$ of amplitude $c_1 = r_0$ with the I–channel of the LCC. Thus the the complex output signal of the LCC is $\tilde{c_1} = r_0 + j0$, as illustrated in Figure 1. Again the corresponding receiver input amplitude is measured:

$$r_1 = \sqrt{(x + r_0)^2 + y^2}. \tag{2}$$

The third step is similar to the second step, except that now we use the LCC to apply a signal of amplitude r_0 to the Q–component only ($\tilde{c_2} = jr_0$), as indicated in Figure 2, and therefore we measure:

$$r_2 = \sqrt{x^2 + (y + r_0)^2}. \tag{3}$$

With these measurements we find the components of the leaking signal by calculating:

$$\begin{aligned} x &= \frac{\frac{1}{2}r_1^2 - r_0^2}{r_0} = \frac{\frac{1}{2}\left(x^2 + 2r_0x + r_0^2 + y^2\right) - r_0^2}{r_0}, \\ y &= \frac{\frac{1}{2}r_2^2 - r_0^2}{r_0}. \end{aligned} \tag{4}$$

At this point we set the LCCs I–channel and Q–channel to $-x$ and $-y$ and in theory achieve perfect cancellation. In practical systems with nonlinear amplitude or power detectors, or changing leakage conditions, the values found by this algorithm are used for a gradient based search algorithm, which were proposed by other authors, for example [7].

In principle, in steps two and three of the proposed algorithm it is not necessary for the probing signal $\tilde{c_1}$ of the LCC to be of amplitude r_0. Any amplitude within the range of the LCC could be used. However, using the same amplitude as the one of the leakage signal $\tilde{r}$ has two benefits: First, and more important, the measured amplitudes in steps two and three r_1 and r_2 will see the most significant change in amplitude, when the probing signal is of amplitude r_0. In the worst case of minimum amplitude change, the probing signal is orthogonal to the leakage signal, so the resulting amplitude is still increased by a factor of $\sqrt{2}$ or $3\,\mathrm{dB}$. Picking larger probing signals will produce larger amplitudes, but these depend less on the leakage signal $\tilde{r}$ we want to measure. This is of special importance, if a logarithmic (power) detector is used, as was done in the practical measurements presented later. The second benefit is the possibility to express x and y in the simple equations (4). When using a different probing amplitude, the calculation of x involves r_0, r_1 and the probing amplitude.

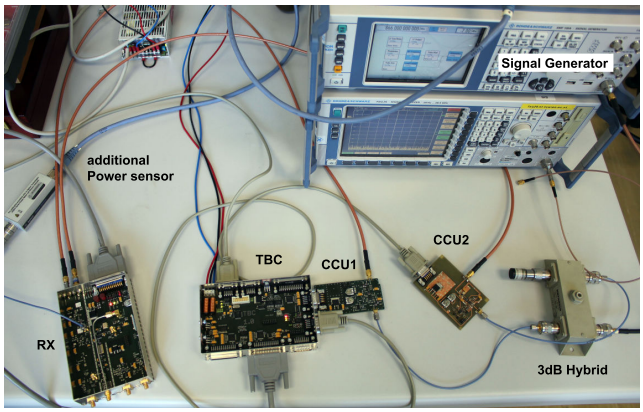

Figure 3. Image showing the measurement setup.

III. Measurement Setup

The measurement setup, which is depicted in Figure 3 is based on our standard RFID testbed hardware described in [11]. The block diagram of the measurement setup is shown in Figure 4. From the receiver of the RFID testbed, only the first part of the frontend is used for these measurements. It contains a bandpass filter suitable for the European RFID UHF band ranging from $865\,\mathrm{MHz}$ to $868\,\mathrm{MHz}$, followed by a directional coupler to add the LCC signal to the received signal. These blocks are followed by a low noise amplifier and a low pass filter. Finally, a directional coupler is used

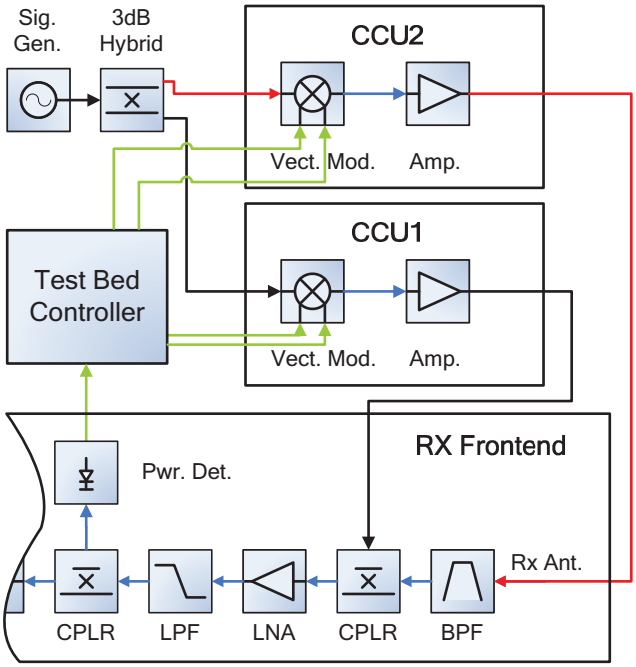

Figure 4. Block diagram of the measurement setup.

to pick a sample of the receiver signal which is fed into a logarithmical power detector. The further signal path of the receiver is not used for these measurements.

The output of the power detector, a LT5537 from Linear Technologies, is connected to a 16-bit Analogue to Digital Converter (ADC) situated in the Test Bed Controller (TBC). The TBC was especially designed to interface the analogue hardware of the RFID testbed and provides a serial RS-232 interface to connect to a standard PC.

For this measurement we do not use a complete RFID measurement system but instead artificially generate the leaking carrier to have full control of the leaking carrier phase and amplitude conditions. Two electrically almost identical modules named CCU1 and CCU2 are used as leaking carrier canceller and artificial leakage generator, respectively. The Carrier Compensation Unit (CCU) is described in [8] and consists of a vector modulator and a power amplifier. The signal from a commercial signal generator operating at 866 MHz is divided in two equal amplitude components by means of a 3 dB–hybrid. The red path in Figure 4, which is controlled by CCU2 generates the artificial leakage signal, which is fed into the receiver input. The cancellation signal generated by CCU1 is fed into the receiver CCU input port which internally connects to the directional coupler described before. Here, the leakage signal and the compensation signal are added up and cancel each other, if CCU1 was properly adjusted.

Both CCUs are controlled by analogue control voltages produced in the TBC. The separate I– and Q–channel inputs are both generated in the TBC using 12-bit Digital to Analogue Converters (DACs). Negative channel settings correspond to DAC values ranging from 0 to 2047, positive settings to DAC values ranging from 2049 to 4095.

An image showing the actual measurement setup is depicted in Figure 3. The additional power sensor shown on the left side of the picture connects to an internal measurement port of the receiver which was used for evaluation and monitoring, only.

IV. Measurements

Before actual measurements were taken, a system calibration is necessary to relate the receiver power detector measurements to vector modulator I/Q–settings.

A. Calibration

The proposed algorithm has several practical benefits, one of them is the possibility to perform the necessary calibration without any additional hardware. The calibration process is necessary to relate receiver power measurements with LCC amplitude settings. With ideal hardware and full system knowledge no calibration is necessary. For real world systems it is necessary to enable the creation of the amplitude calibrated probing signals used in steps two and three of the algorithm, and for correct creation of the compensation signal calculated according to (4).

The only necessary condition for calibration is the absence of an input signal at the receiver antenna input connector, which can be realised by manually disconnecting the antenna or implementing a simple switch to electrically detach the antenna. For the artificial leakage we are using in the specific measurement system described before, CCU2 is simply switched off during calibration.

For the actual calibration, the TBC performs separate sweeps of the I– and Q–channel of the leaking carrier canceller CCU1 and records the power meter readings, while the unswept channel is set to zero output. For the results presented here, the sweeps were conducted in decimal steps of 10 of the DACs and the measured power values were converted to numbers proportional to signal amplitudes. These values are stored in a look–up–table and with the aid of interpolation the necessary DAC values for the LCC signals c_i used in Section II are found.

One additional benefit of this algorithm is, that an actual correspondence to leakage input amplitudes is not necessary, as the gain of the frontend and coupler losses do not appear in the calculations to get the corresponding LCC settings. In truth this calibration routine in combination with the proposed algorithm does not try to detect the input leakage signal, but rather directly produces the optimum I– and Q–settings for the LCC. This is especially valuable, since usual readers allow the user to connect unspecified antennas through cables of unspecified length and loss. Both conditions do not influence the calibration discussed here.

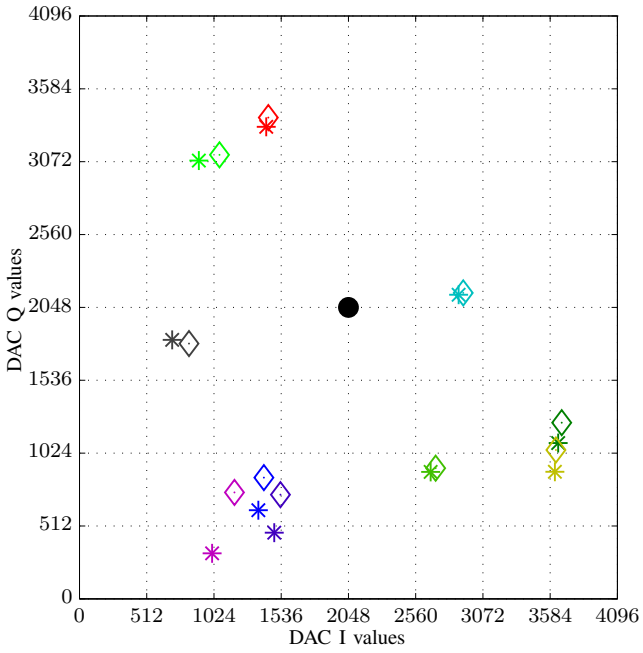

Figure 5. DAC output values of alignment runs performed for 10 arbitrary chosen leakage signals, showing the output of the proposed algorithm as diamonds and the value found by the gradient algorithm as stars.

B. Random artificial leakage measurements

Ten individual measurements were taken, based on an arbitrary chosen leakage signal. A standard PC running Matlab software controlled the TBC and performed the necessary calculations, and was used to store the measurement results. The leakage signal was first generated by setting CCU2 to arbitrary I– and Q–values. Then, the proposed algorithm was used to find the proper I– and Q–setting of the CCU1 acting as LCC. Finally, a gradient based algorithm was used to find the LCC settings with the lowest input power indicated by the receiver power detector. The results are depicted in Figure 5. The setting of the DAC corresponding to zero CCU1 output is located in the middle of the diagram, represented by the black dot at value 2048. The diamond shaped markers indicate the positions found by the three step algorithm, while the star shaped markers indicate the "true" positions found by the gradient algorithm. It is evident from the figure, that the fast algorithm gives a very good starting point for a gradient search algorithm, in some cases the fast algorithm alone might even be sufficient to give reasonable leakage suppression. In the presented ten measurements, the isolation gain

$$G_{\mathrm{I}} = \frac{r_0^2}{|x + jy + c_{\mathrm{FA}}|^2} \tag{5}$$

is ranging from 7.2 dB to 39.7 dB, where c_{FA} is the complex cancellation signal found by the fast algorithm. The average isolation gain is 16 dB.

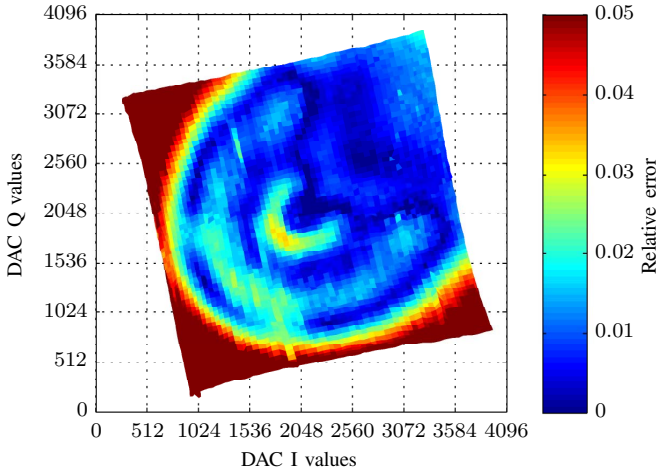

Figure 6. Relative error of the proposed algorithm, plotted over the I/Q-setting space of the LCC (CCU1).

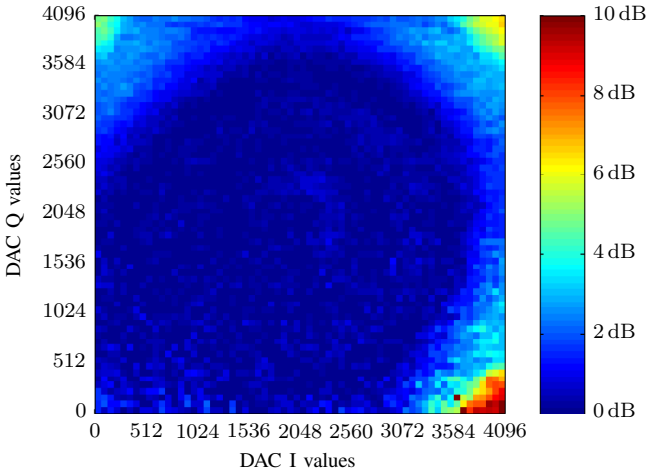

Figure 7. Compensation gain offset error of the proposed algorithm, when compared to the gradient algorithm, plotted over the I/Q-setting space of the artificial leakage signal (CCU2).

C. Systematic artificial leakage measurements

In a second measurement run, a systematic parameter sweep of the artificial leakage signal generated by CCU2 was conducted. In total 4225 points were measured. At each point, the proposed fast algorithm was used and its compensation performance measured. Then a gradient search algorithm was used to find the optimum setting of the LCC. Afterwards, a pure gradient based search algorithm was used to again find the optimum LCC setting. For both methods the numbers of steps needed were recorded.

Figure 6 is a pseudo-colour plot showing the relative error in DAC values of the fast algorithm when compared to the optimum settings found by the gradient algorithm. The plots

axes are with respect to the I/Q space of the LCC. The input amplitude of the artificial leakage signal is slightly smaller than the maximum cancellation amplitude provided by the LCC – thus the coloured square indicating final DAC settings of the LCC which are optimum to compensate for the leakage signals of CCU2 lies within the full range of the LCC constituted by CCU1. Due to uneven propagation time in the cabling of the measurement setup, there is a phase shift between CCU1 and CCU2, which corresponds to the rotation of the square in Figure 6. The colour in this plots indicates the relative error in DAC steps of the fast algorithm when compared to the final results of the gradient search algorithm. For small input signals the error of the fast algorithm is very low and typically below 3%. This is valid for 68% of the points measured in this systematic scan. As mentioned in Section III, a logarithmical power detector is used throughout the measurements. Its output is converted to amplitude values applying an exponential function. Imperfections in the detector response directly translate to errors in the calculated amplitude values. Additionally, the nature of the logarithmic detector reduces the accuracy on a linear scale for large input amplitudes.

For large leakage signals, the imperfect amplitude detector leads to errors of 5% and more in leakage estimation, which can be found on the outer areas in Figure 6. Due to the implementation of the algorithm which solely uses positive probing signals, leakage signals which lie in the negative I/Q–quadrant lead to small amplitude values in the steps two and three of the algorithm. This leads to less errors in the amplitude measurements, and this is why Figure 6 shows low errors in the right top quadrant. Thus, the performance of the algorithm in this practical scenario can be improved by performing steps two and three with positive and negative probing signals, and in each case picking the one with the smaller resulting amplitude to get less amplitude error and better estimation results for large leakage amplitudes of arbitrary phase.

Figure 7 shows a pseudo-colour plot representing the ratio of the resulting power after applying the fast algorithm, and the power resulting on when using the optimum cancellation setting of the gradient algorithm. The axes are with respect to the DAC I/Q–settings of the artificial leakage signal generating vector modulator CCU2 — thus filling the complete I/Q–space which was systematically scanned. The top right corner of Figure 6 corresponds to the bottom left corner in Figure 7, since the compensating signal is the inverted leakage signal, plus the small phase shift introduced by the different path delays in the cables of the measurement setup. For the vast majority of leakage signals the fasts algorithms compensation performance is only $4\,\mathrm{dB}$ or less worse than the optimum setting found by the gradient search. Again some degradation in three of the four corners of Figure 7 is found, which is due to the imperfect amplitude measurements for large signals.

Averaging over all 4225 points, the gradient algorithm required 25.0 steps to reach the optimum value. With the aid of the fast algorithm, only 6.0 additional steps were needed in average to reach the optimum setting. This value could be further lowered by reducing the effects of large signal amplitude measurement errors, either by using a (more) linear detector, or by exploiting positive and negative probing signals, as was described before. Note that each step of the gradient algorithm requires probing measurements similar to steps two and three of the fast algorithm, so that the penalty for using the fast algorithm as a starting point for the gradient search corresponds only to a single additional step of the gradient algorithm.

D. Typical RFID antenna scenario

To verify that the proposed fast algorithm also works in a real–life scenario, the artificial leakage generation was replaced by an RFID antenna scenario, either using a single antenna and a circulator, or using two separate antennas. This was done by using the same measurement setup as depicted in Figure 4, but with CCU2 removed and replaced with either two commercial RFID antennas oriented parallel to each other, or by using a single antenna and a circulator directly attached to it. In both cases the output of the $3\,\mathrm{dB}$–hybrid was additionally fed into a power amplifier which provided $25\,\mathrm{dB}$ of gain, before the transmit signal was routed to the transmit antenna. For each antenna scenario three orientations of the RFID antennas were evaluated, named A–C. In scenario A both antennas faced the wall of the laboratory room bearing windows, in scenario B both antennas faced a metal shelf at the narrow side of the laboratory room, and in scenario C both antennas faced the wall opposite the windows. For the single antenna case the same is true for the single antenna.

The results are summarized in Table I. The second and third columns present the isolation gains G_I for the case of solely using the fast algorithm ($G_{\mathrm{I}_{\mathrm{Fast}}}$), and using a gradient algorithm ($G_{\mathrm{I}_{\mathrm{Grad.}}}$), no matter if aided by the fast algorithm or not, respectively. The isolation gains were calculated from two power measurements conducted with the additional power sensor depicted in Figure 3, which is connected to a measurement output of the receiver frontend. It is noted, that for the dual antenna scenarios A and C the fast algorithm performs even slightly better than the gradient based algorithm. The authors consider this as a coincidence, maybe caused by people acting as scatterers which were moving in the adjacent rooms while the measurement was running. The single antenna scenario showed less isolation than the dual antenna case, as can be expected from literature [12]. As explained in Section IV-C, in our implementation large signals lead to larger errors of the fast algorithm's cancellation signal, which causes the lower isolation gains of the fast algorithm for these scenarios.

In the last two columns of Table I, we compare the

Table I
COMPARISON OF THE ISOLATION GAINS AND NUMBERS OF STEPS REQUIRED FOR THE FAST ALGORITHM AND A CONVENTIONAL GRADIENT ALGORITHM FOR SINGLE AND DUAL ANTENNA SCENARIOS.

Scenario	$G_{\mathrm{I}_{\mathrm{Fast}}}$	$G_{\mathrm{I}_{\mathrm{Grad.}}}$	# Fast	# Fast + Grad.
Dual ant. A	16.4 dB	14.7 dB	10	13
Dual ant. B	15.3 dB	16.1 dB	6	32
Dual ant. C	27.9 dB	24.6 dB	6	31
Single ant. A	8.1 dB	23.9 dB	19	45
Single ant. B	18.2 dB	23.7 dB	7	34
Single ant. C	18.1 dB	24.7 dB	6	38

numbers of steps required for for the gradient algorithm to reach the compensation performance indicated in column three, either when aided by the starting value from the fast algorithm, or when starting from zero in the I/Q–plane. For all cases the fast algorithm aided gradient search needs less steps than the pure gradient algorithm, which reflects the results of the systematic artificial leakage signal presented in Section IV-C.

V. CONCLUSION

In this contribution we present a fast algorithm for leaking carrier canceller alignment. While conventional adjustment procedures usually rely on gradient based search algorithms requiring many steps, the proposed algorithm calculates the optimum LCC setting from three scalar measurements. No additional hardware is necessary, neither to employ the proposed technique, nor to use the proposed self–calibration. An experiment with our RFID testbed proofs the practical usability of the algorithm, and isolation gains up to 39.7 dB were reached. Further isolation improvement is possible by applying some conventional fine adjustment algorithm. In this configuration, the number of steps required for the gradient search on average is reduced by 76%.

REFERENCES

[1] K. Finkenzeller, *RFID Handbook*, second edition ed. Wiley, 2003.

[2] P. V. Nikitin, K. Rao, and R. Martinez, "Differential RCS of RFID tag," *Electronics Letters*, vol. 43, no. 8, pp. 431 – 432, Apr. 2007.

[3] Y. Liu, Q. Zhang, and M. Zheng, "Signal analysis and design criteria for UHF RFID reader," *ITS Telecommunications Proceedings*, pp. 233–236, Jun. 2006.

[4] J.-P. Curty, M. Declercq, C. Dehollain, and N. Joehl, *Design and Optimization of Passive UHF RFID Systems*, 1st ed. Springer, 2007.

[5] T. I. Al-Mahdawi, "Adaptive coherent RFID reader carrier cancellation," U.S. patent US 2006/0183454 , filed Aug. 17, 2006.

[6] D. P. Villame and J. S. Marciano, Jr., "Carrier suppression locked loop mechanism for UHF RFID readers," in *IEEE Int. Conf. on RFID*, Apr. 2010, pp. 141–145.

[7] I. Mayordomo and J. Bernhard, "Implementation of an adaptive leakage cancellation control for passive UHF RFID readers," in *IEEE Int. Conf. on RFID*, Apr. 2011, pp. 121–127.

[8] G. Lasser, R. Langwieser, and A. L. Scholtz, "Broadband suppression properties of active leaking carrier cancellers," in *IEEE Int. Conf. on RFID*, Orlando, USA, April 2009.

[9] R. Langwieser, G. Lasser, C. Angerer, M. Fischer, and A. L. Scholtz, "Active carrier compensation for a multi-antenna RFID reader frontend," in *2010 IEEE MTT-S International Microwave Symposium Digest*, Anaheim, CA, May 2010, pp. 1532–1535.

[10] Impinj, Inc., *Indy® R2000 Reader Chip (IPJ-R2000)*, rev. 1.3 ed., Jul. 2012.

[11] R. Langwieser, G. Lasser, C. Angerer, M. Rupp, and A. L. Scholtz, "A modular UHF reader frontend for a flexible RFID testbed," in *The 2nd Int. EURASIP Workshop on RFID Technology*, Budapest, Hungary, Jul. 2008.

[12] R. Langwieser, G. Lasser, A. L. Scholtz, and M. Rupp, "Comparison of multi-antenna configurations of an RFID reader with active carrier compensation," in *2011 IEEE International Conference on RFID-Technologies and Applications (RFID-TA)*, Sitges, Spain, September 2011, pp. 109–114.